Theoret. Comput. Fluid Dynamics (2000) 13: 327–347

Theoretical and Computational Fluid Dynamics

Simple Shear Flow of Suspensions of Elastic Capsules*

G. Breyiannis and C. Pozrikidis

University of California, San Diego,
La Jolla, CA 92093-0411, U.S.A.
cpozrikidis@ucsd.edu

Communicated by J.R. Blake

Received 26 April 1999 and accepted 5 October 1999

Abstract. The simple shear flow of homogeneous suspensions of two-dimensional capsules enclosed by elastic membranes is studied in the limit of vanishing Reynolds number, in the special case where the viscosity of the fluid enclosed by the capsules is equal to the viscosity of the ambient fluid. The deformation of capsules with circular, elliptical, and biconcave unstressed shapes, and the rheological and statistical properties of their infinitely dilute and moderately dense suspensions are investigated by dynamical simulation using the method of interfacial dynamics for Stokes flow. In a preliminary investigation, the behavior of solitary capsules suspended in an infinite fluid is studied as a function of the dimensionless membrane elasticity number expressing the capsule deformability or the strength of the shear flow. It is found that a critical elasticity number above which a capsule exhibits continued elongation does not exist, and an equilibrium configuration is reached no matter how large the shear rate, in agreement with previous results for three-dimensional flow. A correspondence is established between the elasticity numbers for two- and three-dimensional flow at which the capsules undergo the same degree of deformation. Simulations of pairwise capsule interceptions reveal behavior similar to that exhibited by liquid drops with uniform surface tension. Because of strong hydrodynamic interactions in two-dimensional Stokes flow, the concept of hydrodynamic diffusivity in the limit of infinite dilution is ill-defined in the absence of fluid inertia. Dynamical simulations of doubly periodic monodisperse suspensions with up to 50 capsules distributed in each periodic cell at areal fractions of 0.25 and 0.40 provide information on the effective rheological properties of the suspension and on the nature of the statistical properties of the particle motion. The character of the flow is found to be intermediate between that of liquid drops and rigid particles, and this is attributed to the membrane deformability and to the ability of the interfaces to perform tank-treading motion. The results are compared with rheological measurements of blood flow with good agreement.

1. Introduction

Considerable progress has been made in the past decade in describing the fluid mechanics of deformable liquid particles and in quantifying the rheological and statistical properties of their suspensions. Much of this progress has become possible thanks to the development of efficient numerical algorithms that allow the simulation of highly deformed particles and systems with a multitude of suspended particles in periodic and wall-bounded flows. The state of the art for suspensions of liquid drops whose interfaces exhibit constant surface tension has been reviewed in two recent articles by Charles and Pozrikidis (1998) and Li and Pozrikidis (1999).

* This research was supported by the National Science Foundation. Acknowledgment is made to the Donors of the Petroleum Research Fund, administered by the American Chemical Society, for partial support.

In practice, the interfaces of deformable particles show a variety of mechanical properties that are not adequately described by uniform surface tension. For example, the presence of surfactants renders the surface tension a function of the local surfactant concentration. Surface tension gradients are responsible for interfacial stresses that may either restrict or promote particle deformation. Moreover, impurities and the formation of interfacial shells due to surface reactions are responsible for interfaces that behave like two-dimensional Newtonian or non-Newtonian Boussinesq fluids (e.g., Scriven, 1960; Edwards *et al.*, 1991). The interfaces of biological cells and other vesicles enclosed by thin membranes consist of single or multiple lipid bilayers that resist changes in area and favor flat shapes (e.g., Lipowsky, 1991). The membrane of the red blood cell, in particular, consists of a lipid bilayer resting on a network of an assortment of proteins (e.g., Mohandas and Evans, 1994). The bilayer is responsible for interfacial incompressibility, and the cytoskeleton is responsible for elastic behavior that causes the cell to assume the unstressed shape of the biconcave disk in hydrostatics. A certain class of cells are enclosed by laminated membranes that are responsible for highly non-Newtonian viscoelastic behavior.

In this paper we study, by numerical simulation, the deformation of two-dimensional elastic capsules in shear flow, and the rheological and statistical properties of their homogeneous suspensions, at vanishing Reynolds number. The capsules are regarded as models of red blood cells, and the suspensions are regarded as models of blood at various levels of red blood cell concentration. The main objective of the simulations is to investigate the properties of blood flow using established methods of microhydrodynamics. Normal blood is a suspension of red blood cells, approximately 45% by volume, with a much smaller percentage of white blood cells and platelets also present in the ambient plasma. The cell interior contains a virtually Newtonian fluid whose viscosity can be as high as ten times that of the suspending plasma. Interfacial incompressibility places a strong constraint on the deformation, but the elastic behavior of the membrane is a dominant property at small deformations rendering the elastic capsule model appropriate as a first approximation.

A considerable body of literature is available on the fluid mechanics of viscous drops and inviscid bubbles, for a broad range of conditions. The behavior of capsules enclosed by elastic membranes, however, differs from that of liquid drops in several important ways. In the case of drops, surface velocity gradients may obtain large values associated with the onset of stagnation points. In contrast, in the case of capsules, large interfacial deformations cause the development of large elastic tensions that restrict the deformation and cause the membrane to exhibit tank-treading motion. Thus, unlike a liquid drop, a circular capsule suspended in simple shear flow rotates as a rigid body independently of the viscosity of the enclosed fluid. A noncircular capsule, however, behaves differently than a rigid particle with the same shape: the tank-treading motion of the membrane accommodates external interfacial tractions by inducing an internal flow that differs from rigid-body rotation.

Previous studies on the behavior of capsules emulating red blood cells have focused on the deformation of solitary capsules subject to a shear or elongational flow. Barthés-Biesel (1980), Barthés-Biesel and Rallison (1981), and Barthés-Biesel and Sgaier (1985) studied the small deformation of capsules with spherical unstressed shapes enclosed by elastic or viscoelastic membranes. Li *et al.* (1988) studied the axisymmetric deformation of capsules in elongational flow and established a critical shear rate for continued deformation leading to infinitely elongated shapes. Pozrikidis (1995), Ramanujan and Pozrikidis (1998), Navot (1998), and Eggleton and Popel (1998) simulated the deformation of elastic capsules with various unstressed shapes in simple shear flow, in the limit of vanishing Reynolds number. Cortez and Varela (1997) considered the diametrically opposite limit of capsules suspended in an inviscid fluid and enclosing another inviscid fluid, with the membrane exhibiting resistance to bending. Pozrikidis (1994) studied the deformation of capsules enclosed by viscous membranes.

To investigate the significance of membrane incompressibility, Pozrikidis (1990), Zhou and Pozrikidis (1995), Kraus *et al.* (1996), and Seifert (1998) studied the deformation of capsules enclosed by incompressible interfaces exhibiting a position-dependent tension, neglecting the membrane elasticity. More recently, Boey *et al.* (1998) and Discher *et al.* (1998) developed a coarse-grained molecular model that permits the direct coupling of classical hydrodynamics to the dynamics of the molecular layers and networks comprising the membrane, in a way that circumvents the use of a macroscopic constitutive equation. The rheology of nondilute suspensions of capsules has not been investigated by previous authors, except in the context of data fitting or phenomenological modeling (Skalak *et al.*, 1989).

The simulation of nondilute suspensions of three-dimensional capsules is prohibited by extraordinary demands on computational time even in the simplest case of constant surface tension (Loewenberg and

Hinch, 1996; Zinchenko and Davis, 1999). As a compromise, we restrict our attention to two-dimensional systems and consider capsules with cylindrical shapes. To assess the physical relevance of the results, we compare the deformation of two-dimensional solitary capsules with the deformation of three-dimensional capsules considered by previous authors and find generally good agreement. Previous studies of suspensions of liquid drops have shown that the rheological and statistical properties of two-dimensional suspensions undergoing simple shear flow are similar in many ways to those of their three-dimensional counterparts. An exception is in regard to the particle self- and gradient-diffusivity. Li and Pozrikidis (1999) pointed out that in two-dimensional flow, and in the limit of infinite dilution, both of these quantities diverge in the absence of fluid inertia. In contrast, the corresponding self-diffusivity of three-dimensional liquid drops is well defined, but the gradient-diffusivity diverges in the absence of physical constraints implemented by renormalization. It should be emphasized, however, that these differences pertain to the advanced statistics of the individual particle motion; low-order statistics and global rheological properties are similar.

2. Problem Formulation

The flow model consists of a doubly periodic monodisperse suspension of neutrally buoyant capsules enclosed by elastic membranes, evolving under the action of an imposed simple shear flow with shear rate k along the x axis, as depicted in Figure 1. The instantaneous geometry of the lattice is determined by two base vectors that are convected like material lines under the influence of the unperturbed shear flow, as will be discussed in Section 4. To define the shear rate k, we decompose the velocity field into a doubly periodic component and a nonperiodic component; the y component of the nonperiodic component vanishes, and the x component is given by $u_x = ky$. The motion of the fluid inside and outside the capsules is governed by the equations of Stokes flow (e.g., Pozrikidis, 1997). Considerations of computational cost require that we restrict our attention to the special case where the viscosities of the encapsulated and ambient fluid are the same.

The velocity is required to be continuous across each interface, but the interfacial traction undergoes a discontinuity given by

$$\Delta \boldsymbol{f} \equiv (\sigma^{\text{Ext}} - \sigma^{\text{Int}}) \cdot \boldsymbol{n} = -\frac{\partial(\gamma \boldsymbol{t})}{\partial l} = \gamma \kappa \boldsymbol{n} - \frac{\partial \gamma}{\partial l} \boldsymbol{t}, \tag{1}$$

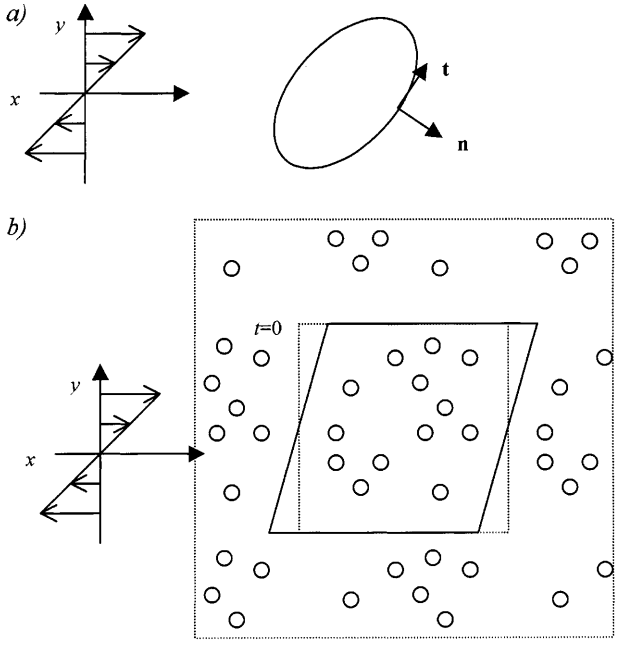

Figure 1. Schematic illustration of (a) a two-dimensional capsule, and (b) a doubly periodic suspension of two-dimensional capsules in simple shear flow.

where σ is the stress tensor, γ is the elastic tension developing due to the deformation, κ the curvature of the interface in the xy plane, $\boldsymbol{n}$ is the normal vector pointing into the external fluid, and l is the arc length along the interface measured in the direction of the unit tangent vector $\boldsymbol{t}$, as shown in Figure 1(a) (e.g., Pozrikidis, 1992). Equation (1) arises from a force balance that neglects the transverse shear tension associated with the bending moment due to the finite thickness of the membrane. The latter can be included by a straightforward modification of the mathematical model under the auspices of the theory of thin shells (Pozrikidis, 1999).

The membrane tension depends on the physical properties of the membrane expressed by an appropriate constitutive equation relating tension to deformation. For small deformations, the tension is a linear function of the stretch or extension ratio ω defined as

$$\omega = \frac{\partial l(t)}{\partial l_0}, \tag{2}$$

where $l(t)$ is the arc length around the interface at time t, and l_0 is the arc length around the interface at the unstressed state denoted by the subscript 0. Thus

$$\gamma = E(\omega - 1), \tag{3}$$

where E is the interfacial modulus of elasticity. When $\omega > 1$, the membane is stretched and the tension is positive; when $\omega < 1$, the membane is compressed and the tension is negative. Although (3) ceases to be accurate when the membrane deformation is not infinitesimal, it continues nevertheless to express the tendency of the membrane to return to the unstressed shape in the absence of flow, albeit in an exaggerated or understated fashion.

Using the well-established formalism of interfacial dynamics for Stokes flow (e.g., Pozrikidis, 1992), we find that the velocity at a point $\boldsymbol{x}_0$ that may lie in the fluid or at a membrane is given by the integral representation

$$u_j(\boldsymbol{x}_0) = u_j^{\infty}(\boldsymbol{x}_0) - \frac{1}{4\pi\mu}\sum_{m=1}^{N}\int_{C_m} \Delta f_i(\boldsymbol{x})\, G_{ij}(\boldsymbol{x},\boldsymbol{x}_0)\, \mathrm{d}l(\boldsymbol{x}), \tag{4}$$

where C_m is the contour of the mth capsule, the summation is over all capsules suspended in a periodic cell, μ is the viscosity of the capsule and ambient fluid, and $\boldsymbol{G}$ is the doubly periodic Green's function of two-dimensional Stokes flow representing the velocity field due to a two-dimensional lattice of point forces (Van den Vorst, 1996; Pozrikidis, 1996).

Rendering all variables dimensionless using as a characteristic length scale the equivalent radius of the capsules a, time k^{-1}, velocity ka, and stress μk, we recast (4) into the form

$$\hat{u}_j(\hat{\boldsymbol{x}}_0) = \delta_{jx}\hat{y} - \frac{1}{4\pi\Omega}\sum_{m=1}^{N}\int_{C_m} \Delta\hat{f}_i(\hat{\boldsymbol{x}})\hat{G}_{ij}(\hat{\boldsymbol{x}},\hat{\boldsymbol{x}}_0)\, \mathrm{d}\hat{l}(\hat{\boldsymbol{x}}), \tag{5}$$

where dimensionless variables are denoted by a caret, and

$$\Omega \equiv \frac{\mu k a}{E}. \tag{6}$$

The dimensionless number Ω is the counterpart of the capillary number for drops with isotropic surface tension, and may be regarded as either an inverse elasticity number or a dimensionless shear rate.

The rheological properties of the suspension are described in terms of flow variables arising by taking spatial averages indicated by angular brackets (Batchelor, 1970). The effective stress tensor is given by

$$\langle\sigma_{ij}\rangle = -\delta_{ij}\langle p\rangle + 2\mu\langle e_{ij}\rangle + \sigma_{ij}^{\mathrm{P}}, \tag{7}$$

where $\boldsymbol{e}$ is the rate of deformation tensor and σ^{P} is the contribution of the suspended particles. In the special case where the viscosity of the capsules is equal to that of the ambient fluid, we find

$$\sigma_{ij}^{\mathrm{P}} = \frac{1}{A}\sum_{m=1}^{N}\int_{C_m} \Delta f_i(\boldsymbol{x}) x_j\, \mathrm{d}l(\boldsymbol{x}), \tag{8}$$

where A is the area of a periodic cell (Pozrikidis, 1992; Kennedy *et al.*, 1994). The integral on the right-hand side is the coefficient of the stresslet in the multipole expansion. Substituting the expression in the middle of (1) into (8), and integrating by parts, we find the computationally convenient form

$$\sigma_{ij}^{\mathrm{P}} = \frac{1}{A}\sum_{m=1}^{N}\int_{C_m}\gamma(\boldsymbol{x})t_i(\boldsymbol{x})t_j(\boldsymbol{x})\,\mathrm{d}l(\boldsymbol{x}) \tag{9}$$

derived previously by Rosenkilde (1967) for interfaces with constant surface tension.

Considering capsules that are suspended in an infinite ambient fluid or in a doubly periodic simple shear flow, we use the divergence theorem and the periodicity condition to find that the spatial average of the rate of deformation tensor $\langle \boldsymbol{e} \rangle$ takes the following familiar form for homogeneous shear flow,

$$\langle \boldsymbol{e} \rangle = \tfrac{1}{2}k\begin{bmatrix} 0 & 1 \\ 1 & 0 \end{bmatrix}. \tag{10}$$

This simplification allows us to describe the rheological behavior of the suspension in terms of the effective viscosity defined as

$$\mu_{\mathrm{eff}} = \frac{1}{2}\frac{\langle \sigma_{12} \rangle}{\langle e_{12} \rangle} \tag{11}$$

and the normal stress difference defined as

$$N = \langle \sigma_{11} \rangle - \langle \sigma_{22} \rangle. \tag{12}$$

In subsequent sections we describe the deformation of an individual capsule in terms of the Taylor deformation parameter D, which is defined in terms of the maximum and minimum capsule dimensions A and B, as $D = (A - B)/(A + B)$. To reduce the sensitivity of these variables to the fine features of the capsule's geometry, we compute A and B by mapping a deformed capsule to an ellipse that shares the tensor of the moments of inertia. The principal direction of this tensor is identified with the capsule inclination.

3. Numerical Method

The numerical method used to simulate the motion of the capsules is similar to that developed by Li *et al.* (1996) and Charles and Pozrikidis (1998) for drops with constant interfacial tension. Each membrane is traced by a set of marker points, and the shape of the membrane is approximated by cubic spline interpolation with respect to the arc length of the polyline connecting successive marker points. The marker points are convected with the velocity of the fluid which is computed using the following discretized form of the integral representation (5):

$$\hat{u}_j(\hat{\boldsymbol{x}}_0) = \delta_{jx}\hat{y} - \frac{1}{4\pi\Omega}\sum_{m=1}^{N}\sum_{p=1}^{K_m}[\Delta\hat{f}_i]_{m,p}\int_{E_{m,p}}\hat{G}_{ij}(\hat{\boldsymbol{x}},\hat{\boldsymbol{x}}_0)\,\mathrm{d}\hat{l}(\hat{\boldsymbol{x}}), \tag{13}$$

where K_m is the number of segments around the mth interface, and the square brackets denote the difference of the values of the enclosed quantity evaluated at the segment end points. As the integration point approaches the point where the velocity is evaluated, the kernel of the single-layer potential exhibits a logarithmic singularity which is subtracted and then integrated analytically over the cubic segments. To compute the stretch ω defined in (2), we introduce the function $l_0(l)$ and compute the requisite derivative $\partial l/\partial l_0$ by cubic spline interpolation with respect to the polygonal arc length.

In the numerical simulations we consider solitary capsules as well as capsules in doubly periodic arrangements. In the case of doubly periodic flow, the evaluation of Green's function consumes the vast majority of the computational effort. Trilinear interpolation of the nonsingular part of Green's function from a prepared look up table with respect to (a) the differences in the Cartesian coordinates of the observation point and the pole, and (b) the convected y coordinate of the second base vector, was used to expedite the simulations.

The size of the interpolation grid was 64^3 yielding a relative error on the order of 10^{-5}. The position of the marker points was advanced in time using the second-order Runge–Kutta method.

A sawtooth-like numerical instability in the distribution of the marker points arises in simulations with strongly interacting capsules. Numerical experimentation showed that increasing the number of marker points while simultaneously reducing the size of the time step ameliorates the instability, but the computations become impractical. As an alternative, we smooth the position of the marker points using a method developed by Dold (1992) which involves fitting a polynomial of $M-2$ order through M consecutive marker points. Assuming a positive displacement due to the instability at even-numbered points, accompanied by a negative displacement at odd-numbered points, the unphysical displacements are removed by rejecting appropriate coefficients of the polynomial and recomputing the marker point coordinates. We found that $M = 15$ suppresses the instability effectively in all cases considered for the duration of the simulation.

To investigate the effect of smoothing, we compared the deformation of a solitary capsule with an elliptical unstressed shape of axes ratio equal to 0.3 computed with and without smoothing, and observed only small differences both in the final equilibrium shapes and in the history of the deformation parameter and capsule inclination. In a more demanding test, we simulated the relaxation of a highly deformed capsule to the unstressed biconcave shape – which is the two-dimensional counterpart of the biconcave disk assumed by red blood cells – and recovered the unstressed profile.

In performing dynamical simulations with closely packed strongly interacting capsules, a small time step is required to prevent artificial interface crossing. As two capsules approach one another, the system of governing equations becomes stiff due to strong lubrication forces developing at the gaps between the membranes. Previous simulations dealt with this difficulty by either introducing a repulsive short-range force or repositioning the interfaces at close contact. We used a combination of a small time step and a large number of marker points. Typically, 20–32 marker points were distributed around each membrane, and the time step was varied in the range of $0.00050k^{-1}$–$0.005k^{-1}$, as necessary, to secure numerical stability. A simulation of a doubly periodic suspension with 50 capsules for a time period of $50k^{-1}$ requires 5–10 hours of CPU time on the Cray T90 of the San Diego Supercomputer Center.

4. Solitary Capsules and Pairwise Interceptions

We carried out an extensive series of simulations of the deformation of solitary capsules with various unstressed shapes. The aims of this prelimnary study were: (a) to obtain estimates for the magnitude of the capsule deformation and inclination in terms of the dimensionless inverse elasticity parameter Ω; (b) to illustrate the rheological properties of dilute suspensions; and (c) to establish the physical relevance of two-dimensional flow by comparing the results with results for three-dimensional flow presented by previous authors.

The numerical results suggest that a solitary capsule with a circular unstressed shape deforms and reaches a steady equilibrium shape for any value of Ω, however large. The more a capsule deforms, the larger the magnitude of the elastic tensions resisting the deformation and leading to an equilibrium configuration. A critical shear rate above which a capsule exhibits continued elongation does not arise, and the aspect ratio of the equilibrium shape is a monotonically increasing function of Ω. This behavior is similar to that of three-dimensional capsules subjected to a simple shear flow, but different than that of axisymmetric capsules subjected to uniaxial extensional flow where a critical value of Ω above which the capsule exhibits continued elongation has been identified (Li *et al.*, 1988; Ramanujan and Pozrikidis, 1998). The equilibrium inclination angle decreases monotonically from 45° for a slightly deformed capsule, to zero for a substantially deformed capsule. Highly elongated capsules tend to align with the streamlines of the incident simple shear flow. Flipping motions similar to those exhibited by rigid particles, or sustained oscillations similar to those exhibited by highly viscous drops, were not observed.

Figure 2(a), (b) shows the evolution of the deformation parameter and inclination angle of capsules with circular unstressed shapes evolving toward the equilibrium shapes, for several values of Ω, and Figure 2(c) shows a collection of equilibrium shapes. Slightly and moderately deformed shapes are elliptical, highly deformed shapes are slender and sigmoidal. These results are qualitatively similar with those presented by previous authors for three-dimensional capsules with spherical unstressed shapes and compact deformed

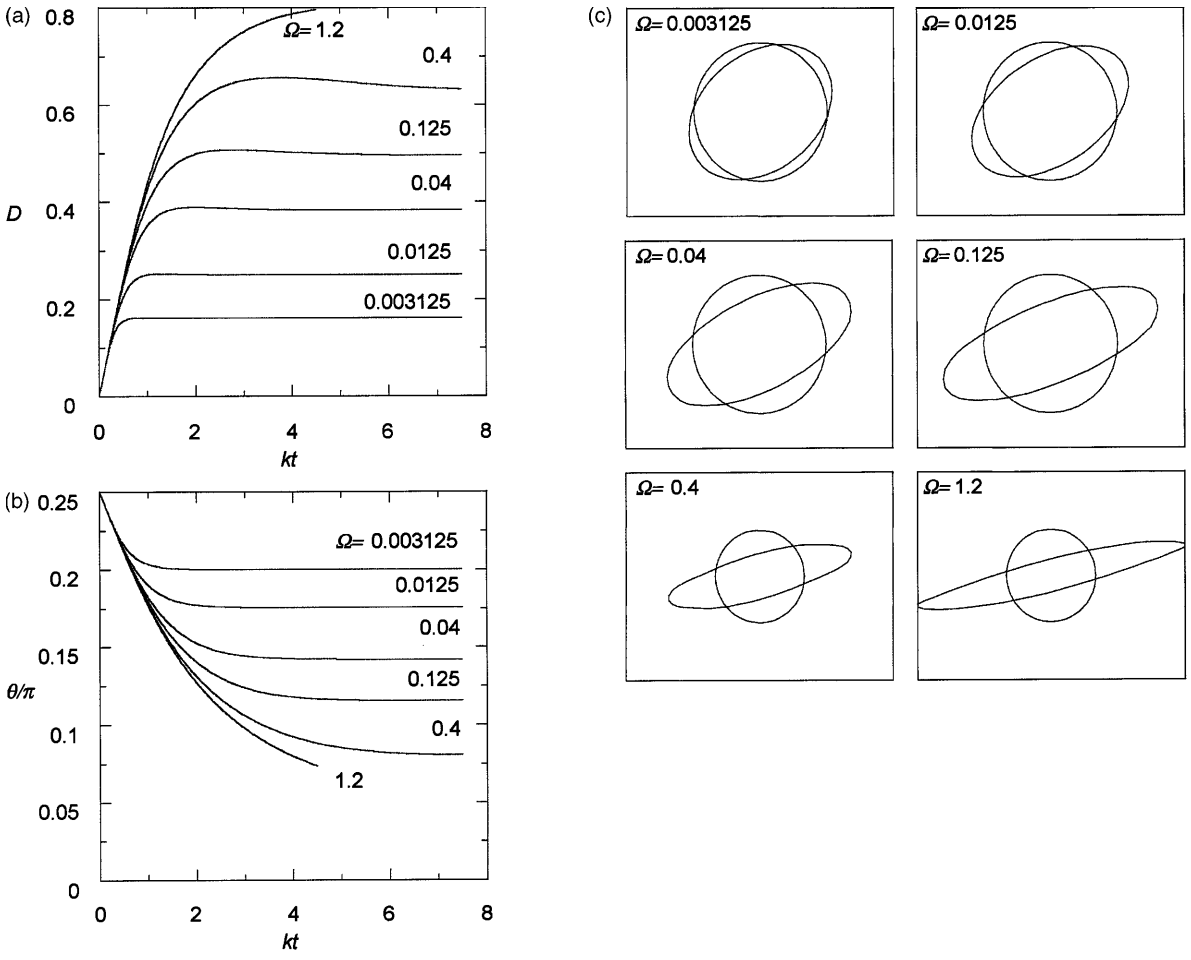

Figure 2. Deformation of solitary capsules with circular unstressed shapes of equivalent radius a. Evolution of (a) the deformation parameter, and (b) inclination angle. (c) Illustration of the circular and deformed membrane profiles at equilibrium, for several values of the dimensionless shear rates Ω = 0.003125, 00125, 0.04, 0.125, 0.4, and 1.2.

shapes. In particular, the traces of three-dimensional capsules at the capsule midplane presented by Ramanujan and Pozrikidis (1998) are strikingly similar to those shown in Figure 2(c). This agreement suggests that near the midplane of a three-dimensional capsule, and far away from the tips, the flow is effectively two-dimensional.

To establish a correspondence between two- and three-dimensional capsules, we identify the respective values of Ω at which the deformation parameters of equilibrium shapes are identical, and plot them against each other in Figure 3. The difference between the two numbers diminishes as the capsule deformation is raised, and there is a particular value of Ω at which the deformations are identical. The function corresponding to the data within the range considered is accurately represented by the empirical polynomial

$$\Omega_{2D} = -0.0084117 + 0.45073\Omega_{3D} + 0.75662\Omega_{3D}^2, \tag{14}$$

which provides us with a basis for interpreting results for two-dimensional flow in the realistic context of three-dimensional flow, in the limit of infinite dilution, and perhaps at moderate concentrations. It should be pointed out, however, that this correspondence is meaningfull only at small and moderate deformations where the capsules have compact shapes. At large shear rates, the differences between two- and three-dimensional flows are substantial.

To study the significance of the unstressed capsule shape, we performed several series of simulations for capsules with elliptical and biconcave unstressed shapes. The biconcave shapes are described in parametric

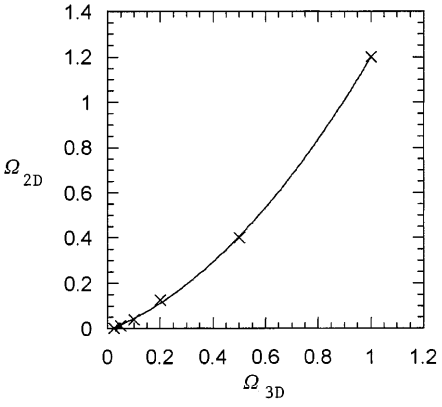

Figure 3. Correlation between the dimensionless shear rate in two-dimensional flow, Ω_{2D}, and the corresponding dimensionless shear rate in three-dimensional flow where the capsules exhibit the same degree of deformation, Ω_{3D}, for capsules with circular or spherical unstressed shapes of radius a. The solid line corresponds to correlation (14).

form by the equations

$$x = \alpha\xi, \qquad y = \tfrac{1}{2}\alpha\sqrt{1-\xi^2}\,(c_0 + c_2\xi^2 + c_4\xi^4), \tag{15}$$

where $-1 \leq \xi \leq 1$, $c_0 = 0.207$, $c_2 = 2.003$, $c_0 = -1.123$, and the scaling factor α is adjusted so that the equivalent radius of the capsule is equal to a. Equation (15) describes the generating contour of normal red blood cells with discoidal shapes (Fung, 1981). In all cases we observed behavior similar to that discussed previously for capsules with circular unstressed shapes, with the equilibrium deformation parameter being a monotonic function of the dimensionless shear rate. The equilibrium deformation parameter, inclination angle, average of the tangential membrane velocity, membrane tank-treading frequency, and effective rheological properties of a dilute suspension are plotted in Figure 4 for elliptical unstressed shapes with four aspect ratios. In all cases, a is the equivalent capsule radius. Note that slightly deformed capsules with noncircular unstressed shapes are oriented at an angle that is less than 45° with respect to the direction of the shear flow.

Figure 4(c) shows that, in the case of circular unstressed capsules, the average value of the tangential membrane velocity tends to $0.5ka$ at small deformations, corresponding to rigid-body rotation. Correspondingly, the tank-treading frequency tends to the reference value of k/π. In the case of noncircular unstressed capsules, the average value of the tangential membrane velocity and the tank-treading frequency take values that are less than these reference values. The effective shear stress and normal stress differences, shown in Figure 4(e), (f), have been reduced by the effective shear stress of an infinitely dilute suspension of rigid circular disks S_D given by $S_D = \gamma\mu_{\text{Eff},D}$, where μ_{Eff} is the corresponding effective viscosity given by

$$\mu_{\text{Eff},D} = \mu(1 + 2\varphi) \tag{16}$$

(Belzons *et al.*, 1981). When the correlation (14) is used, the deformation of the capsules and the rheological properties of the suspension agree well with the values reported by Ramanujan and Pozrikidis (1998) for three-dimensional capsules with spherical unstressed shapes. Both two- and three-dimensional suspensions exhibit shear-thinning and some type of elastic behavior.

Animation showed that at small and moderate values of Ω, the transient deformation from the unstressed to the equilibrium shape occurs monotonically through gradual extension. At high values of Ω, this transition proceeds through a rapid initial deformation followed by relaxation to a sigmoidal shape, as shown in Figure 5(a). This is also evident in the overshooting of the deformation parameter and inclination angle plotted in Figure 5(b), (c) for elongated capsules with various unstressed shapes. The simulations showed that the highly curved tips of highly elongated capsules oscillate between pointed and rounded shapes, as manifested by the small-amplitude undulations of the inclination angle shown in Figure 5(d), (e). This oscillation, however, was confirmed to be a numerical artifact associated with smoothing. The developing elastic interfacial tensions are strong functions of the position of the marker points, and small displacements due to numerical error generate flows that cause the interface to cross streamlines emanating from stagnation points established near the interface. For illustration, the instantaneous streamline pattern in the vicinity of an elongated tip is shown in Figure 5(f).

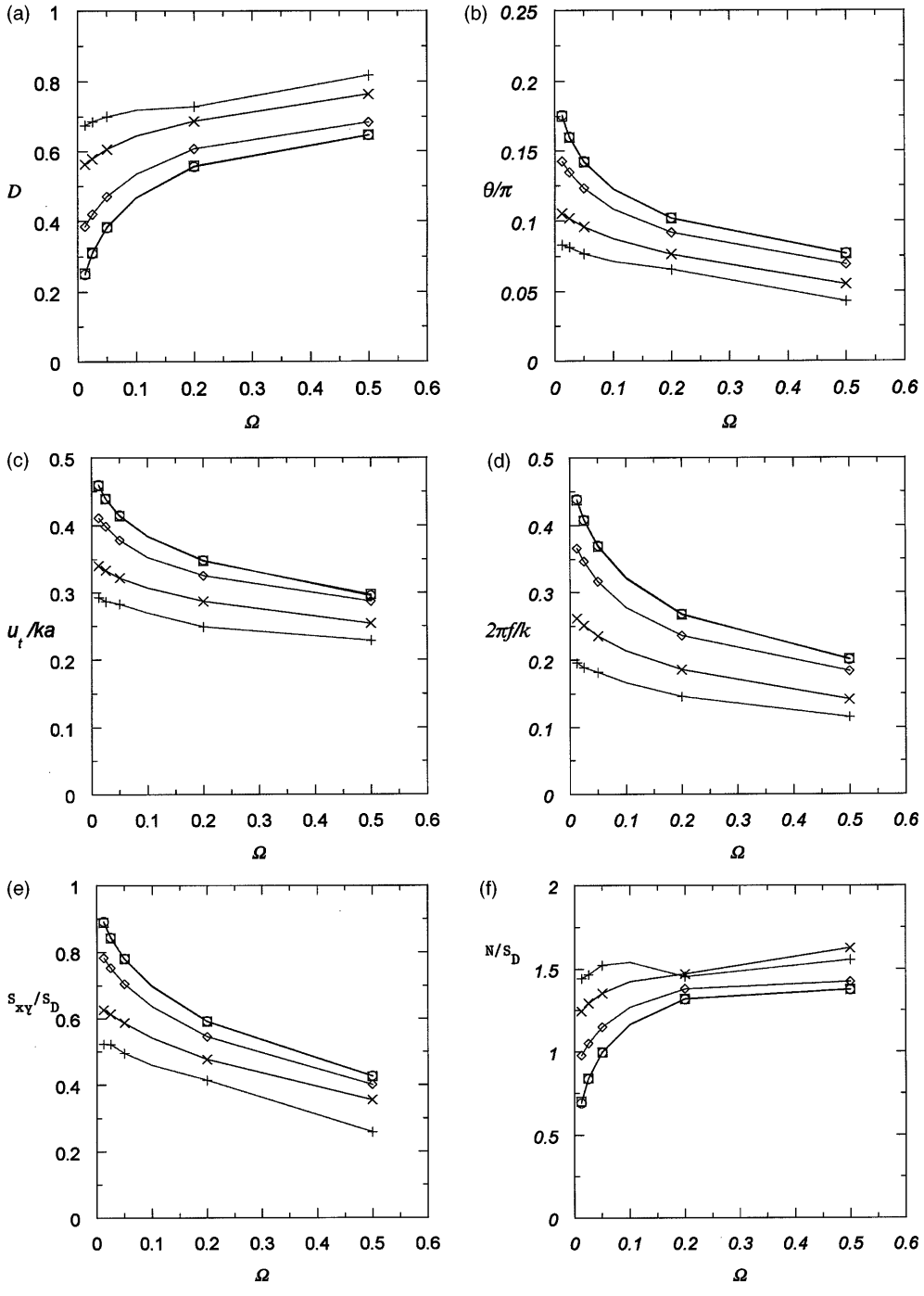

Figure 4. Deformation of solitary capsules with circular, elliptical, and biconcave unstressed shapes. Geometrical and rheological properties at equilibrium as functions of the dimensionless shear rate $\Omega = \mu Ga/E$, where a is the equivalent capsule radius. (a) Deformation parameter, (b) inclination angle, (c) average tangential velocity, (d) tank-treading frequency, (e) shear component of the particle stress tensor reduced by that for a solid disk, and (f) reduced normal stress difference. ○, circular unstressed capsules; □, elliptical unstressed capsules with axes ratio 0.9; ♢, elliptical unstressed capsules with axes ratio 0.5; + elliptical, and ×, biconcave unstressed capsules described by (15).

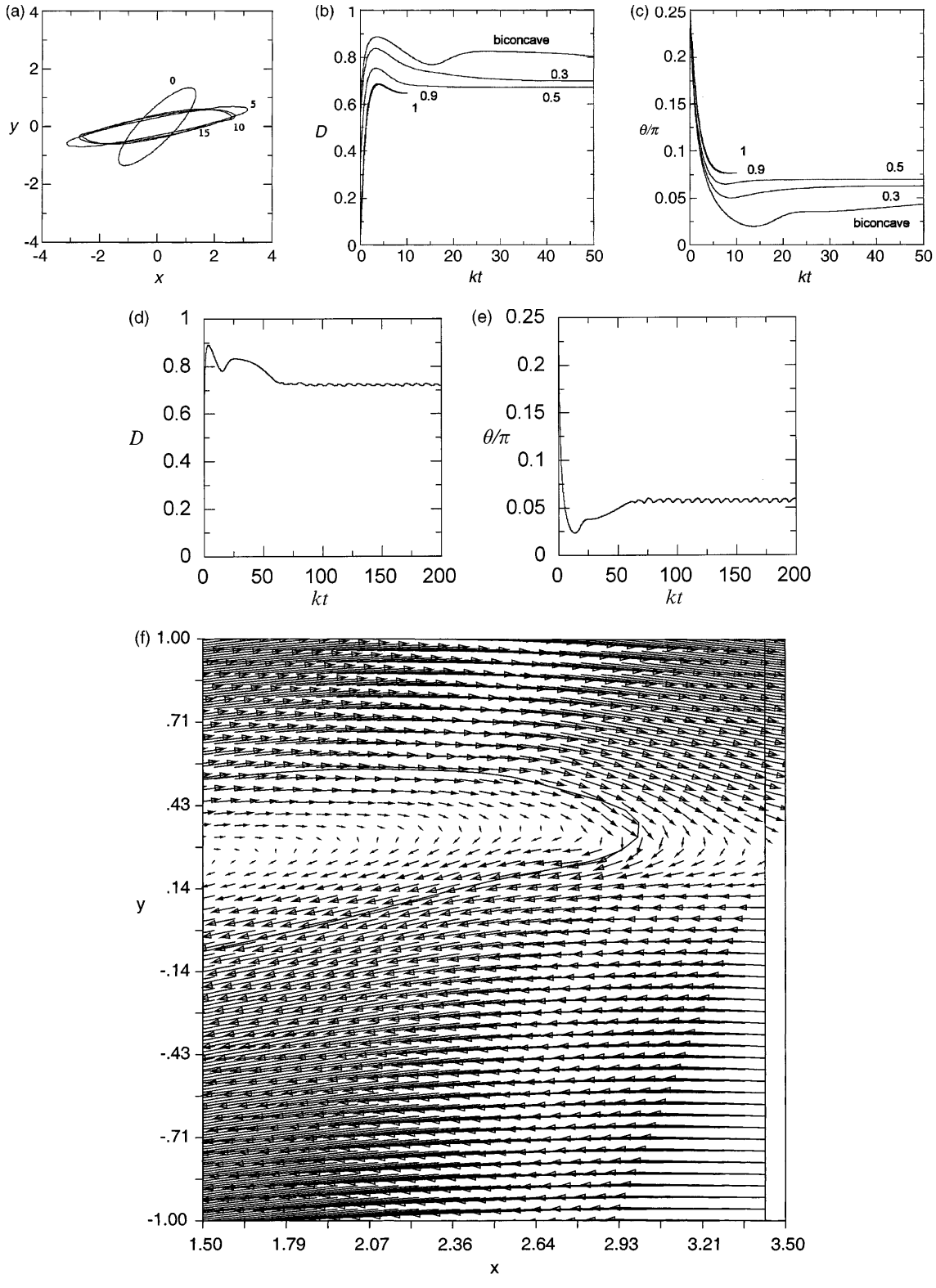

Figure 5. (a) A sequence of deforming profiles of a capsule showing the initial extension and subsequent relaxation to the equilibrium shape. The labels show the dimensionless time kt. (b, c) Evolution of the deformation parameter and orientation angle of elastic capsules with various unstressed shapes at $\Omega = 0.5$. The curve labels are the axes ratio of capsules with elliptical unstressed shapes. (d), (e) Long-time evolution of the biconcave capsules. The low-amplitude oscillations at long times are due to numerical instabilities. (f) The flow field near the tip of a highly deformed elastic capsule with a biconcave unstressed shape at $\Omega = 0.5$, at time $kt = 45$.

Pairwise Interception

During the flow of a moderately dense suspension, two capsules occasionally intercept one another suffering temporary rotation and deformation. After the pairwise interaction has ended, the capsules exhibit a net lateral displacement δ that is a function of the initial lateral separation. To develop insights into the nature of this interaction, we simulated the interception of two capsules of equal size in infinite shear flow. At the initial instant, the capsules have the equilibrium shapes of deformed solitary capsules, and their centers are separated by the horizontal distance $40a$ in the direction of the unperturbed shear flow, and by the vertical distance Δy normal to the streamlines of the unperturbed shear flow; a is the equivalent capsule radius. The results of these simulations are similar to those reported by previous authors for liquid drops with constant surface tension (e.g., Li and Pozrikidis, 1999).

In Figure 6, we plot the net displacement δ, against the initial vertical separation Δy on a log-log scale. The data confirms that, for large values of Δy, δ decays as Δy^{-1}, which is consistent with the point-force-dipole-like decay of the velocity field due to a force-free particle. Using the theory of random walks, we can express the self-diffusivity of a particle in a homogeneous dilute suspension and the gradient-diffusivity of a particle in an inhomogeneous dilute suspension, in terms of integrals of δ with respect to Δy. Li and Pozrikidis (1999) noted that, in the case of droplets with constant surface tension, the slow decay of δ with respect to Δy, due to far-reaching hydrodynamic interactions, causes both of these diffusivities to diverge and render the concept of Fickian diffusivity poorly defined. Their discussion is also applicable to the present case of elastic capsules.

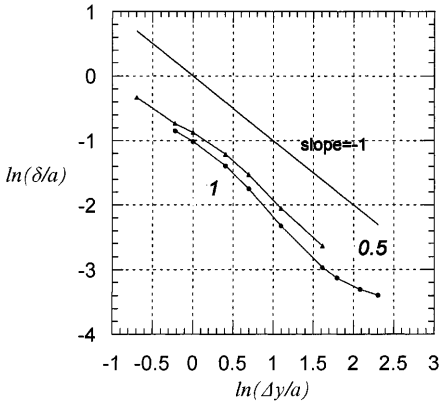

Figure 6. Net displacement of two capsules with eliptical unstressed shapes after interception in infinite shear flow, plotted as a function of the initial lateral separation, for $\Omega = 0.01$. The curve labels are the axes ratios in the unstressed state.

5. Dense Suspensions in a Double Periodic Arrangement

To investigate the flow of nondilute suspensions, we consider a doubly periodic monodisperse suspension of N capsules randomly distributed within each periodic rectange, as discussed in Section 2. The suspension evolves under the influence of a simple shear flow directed along the x axis, as depicted in Figure 1(b). The areal fraction of the capsules is $\varphi = N\pi a^2/A$, where A is the preserved area of the computational unit box, and a is the equivalent radius of each capsule. At any instant, the periodic structure of the suspension is defined by two base vectors $\boldsymbol{a}_1$ and $\boldsymbol{a}_2$. The first base vector $\boldsymbol{a}_1$ is stationary and remains oriented along the x axis; the second base vector $\boldsymbol{a}_2$ evolves as though it were a material vector being stretched under the action of the unperturbed simple shear flow.

We carried out a number of exploratory simulations of circular and elliptical unstressed capsules at moderate and high volume fractions. To investigate the effect of the unstressed shape, we carried out two main series of simulations of 50 suspended capsules of equivalent radius $a = 0.040A^{1/2}$, corresponding to the areal fraction $\varphi = 0.25$, for $\Omega = \mu ka/E = 0.004$. The initial capsule position and orientation were determined by a random-number generator, with care taken to prevent overlap.

Figure 7(a) shows typical interfacial profiles developing during the evolution of a suspension of capsules with circular unstressed shapes, at times $kt = 0$, 20, 50. Figure 7(b) displays corresponding profiles of

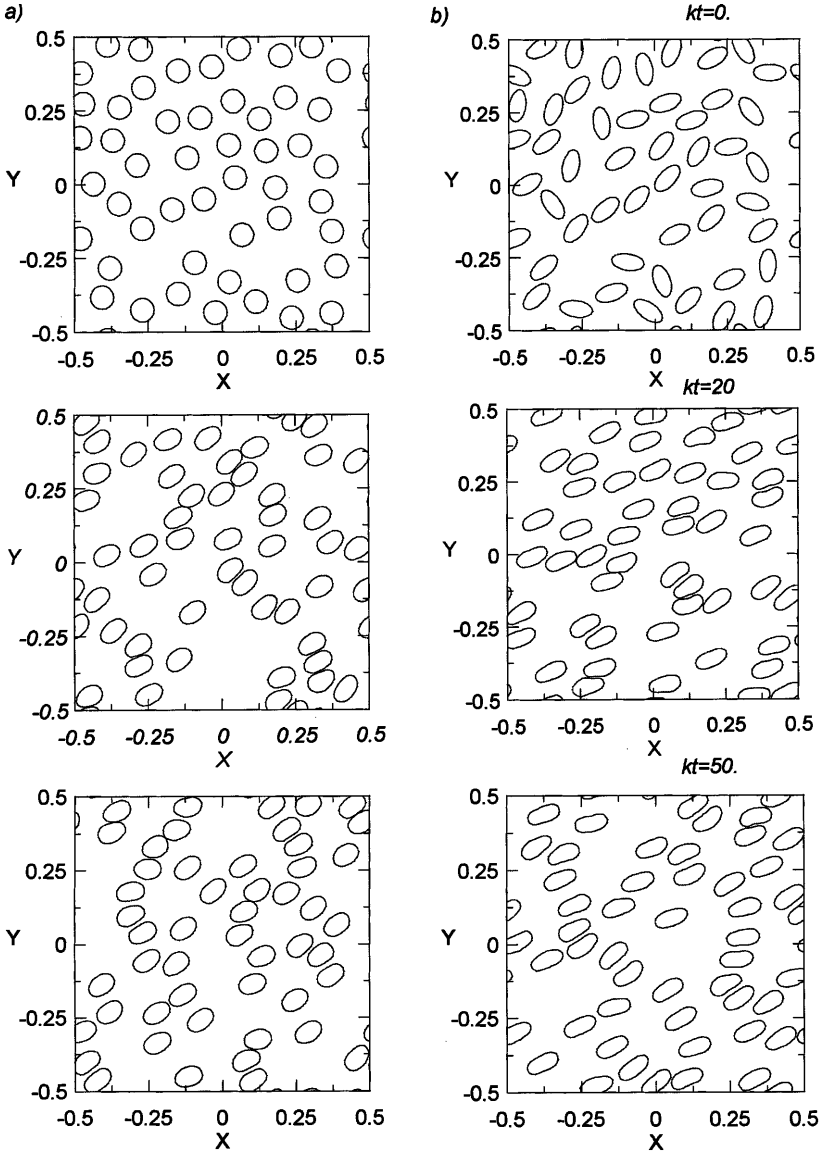

Figure 7. Interfacial profiles developing during the evolution of a suspension of 50 elastic capsules, at areal fraction $\varphi = 0.25$, for $\Omega = 0.04$, at times $kt = 0$, 20, and 50. (a) Circular unstressed shapes, and (b) elliptical unstressed shape with axes ratio 0.5.

capsules with elliptical unstressed shapes with axes ratio 0.5. In both cases, after a transient start-up period, the capsules orient themselves at an angle that is less than 45° with respect to the direction of the incident shear flow, while developing wobbly shapes, and then start interacting while convected under the action of the simple shear flow. The average deformation parameter is around 0.22 for circular capsules and around 0.356 for elliptical capsules. Although the sequence of illustrations in Figure 7(a), (b) presents evidence of temporary formation of aggregates, a pronounced tendency for cluster formation is not apparent. The tank-treading motion of the interfaces allows the capsules to slide over each other and prevents the onset of strong lubrication forces responsible for cluster formation in sheared suspensions of solid particles (Brady and Bossis, 1985).

We have examined the evolution of the y coordinate of one marker point over each one of the 50 simulated capsules, shifted by its initial position. During the initial start-up period, we observed a synchronous sinusoidal oscillation corresponding to uniform tank-treading motion. At later times, the random motion causes significant dispersion. The average frequency of the trank-treading motion was found to be close to the value for solitary capsules shown in Figure 4(d) for $\Omega = 0.004$, and lies in the range reported

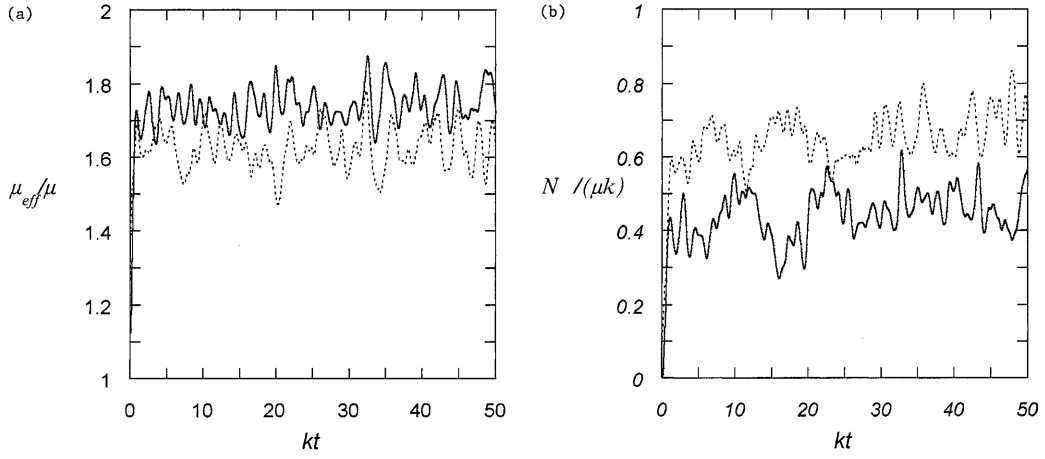

Figure 8. Evolution of the reduced effective viscosity and normal stress difference of the suspensions depicted in Figure 7.

by Ramanujan and Pozrikidis (1998) for three-dimensional solitary capsules. The values for the elliptical unstressed capsules are lower than those for the circular capsules due to the increased length of the interface.

In Figure 8 we plot the evolution of the effective viscosity μ_{eff} and normal stress difference N defined in Section 2 for the suspensions depicted in Figure 7. After a short period of initial adjustment, both variables rise from the initial values of unity or zero and fluctuate around well-defined mean values, suggesting that the flow reaches a state of statistical equilibrium. Comparing the results for circular unstressed shapes, plotted with the solid line, to the results for elliptical unstressed shapes, plotted with the dashed line, we note that the fluctuations have comparable magnitudes but the mean values are significantly different. The effective viscosity for elliptical capsules is lower than that for circular capsules due to the diminished intensity of the perturbation caused by their presence: a flat capsule aligns with the shear flow while the membrane executes tank-treading motion with a tangential velocity that is equal to the local velocity of the shear flow. The analysis for infinitely dilute suspensions of circular rigid particles predicts $\mu_{\text{eff}} = 1.5\mu$, which lies below the mean values for both circular and elliptical capsules. In contrast, the normal stress differences for elliptical capsules is higher than that for circular capsules due to the geometrical anisotropy of the dispersed phase. Overall, the rheological properties of suspensions of elastic capsules are found to be similar to those of liquid drops, in the sense that both are determined by the particle elongation and inclination, with particle clustering playing only a minor role.

The dynamics of the microstructure of the evolving suspension may be described in terms of the particle-center pair distribution function $g(r, \theta)$, where r is the distance of the designated center of a particle from the designated center of another test particle, and θ is the corresponding polar angle (e.g., Hansen and McDonald, 1986). The function $g(r, \theta)$ is defined as the probability of finding a particle within the differential area $r\,\mathrm{d}r\,\mathrm{d}\theta$ centered at the position (r, θ), divided by the corresponding probability when the particle distribution is homogeneous. In a periodic suspension, as the number of particles in an ensemble tends to infinity, and as the distance r/a tends to infinity, the function g tends to the value of unity at any angle θ. The information carried by the pair distribution function is sufficient for characterizing the geometry of the microstructure as well as for identifying the spontaneous formation of doublets or higher-order particle clusters due to the flow (Russell *et al.*, 1989, pp. 264–267)

In Figures 9 and 10 we present graphs of the pair distribution function averaged over time for several angles θ, plotted as a function of the distance r/a. In the case of circular unstressed capsules, corresponding to Figure 9, the pair-distribution function peaks at a certain distance, and then falls off gradually to the asymptotic value of unity exhibiting mild fluctuations. Because of the interfacial deformability, there is a nonzero probability that two particles are located closer than two equivalent radii. Closer examination reveals that the peaks for $\theta = 0$ and π are located near the rigid-particle limit of two times the equivalent capsule radius, and are shifted to higher values for intermediate angles. The peak is highest for $\theta = 5\pi/6$ and lowest for $\theta = \pi/6$ which are close, respectively, to the angles corresponding to the directions of the compressive and extensional axes of the simple shear flow. Overall, the graphs in Figure 9 suggest that particles tend

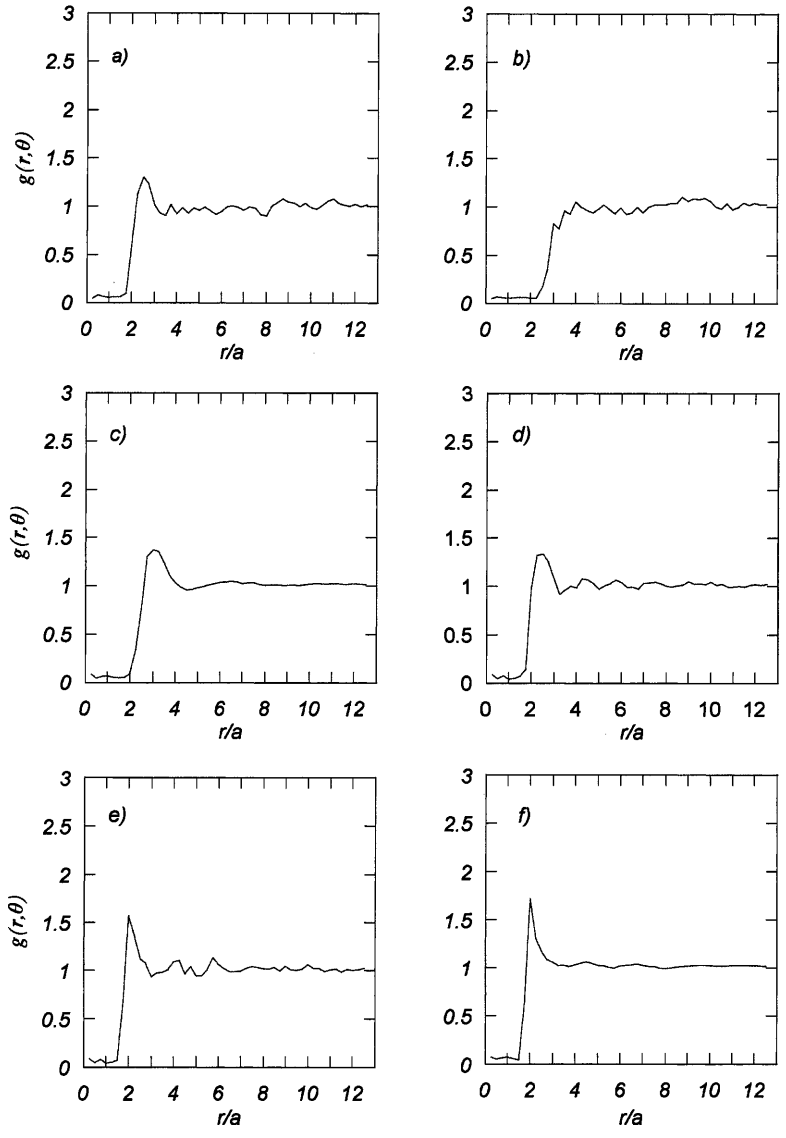

Figure 9. Pair-distribution function g plotted against the radial distance r/a for various angular positions corresponding to the suspension depicted in Figure 7(a); (a) $\theta = 0$, (b) $\pi/6$, (c) $\pi/3$, (d) $\pi/2$, (e) $2\pi/3$, and (f) $5\pi/6$.

to form doublets over a wide range of orientations. The occurrence of weak fluctuations indicates a weak tendency for cluster formation.

A substantially different behavior is observed for elliptical particles, as shown in Figure 10. The peaks are only moderate, and the dependence of g on θ is stronger. In fact, peaks are discernible only in directions that are close to the horizontal, and this reveals a mild tendency of the capsules to form pairs in the streamwise direction. These predictions are consistent with the instantaneous profiles shown in Figure 7.

Previous experimental and numerical work has suggested that the seemingly random motion of a tagged particle in a homogeneous suspension of rigid particles or liquid drops may be described in terms of a hydrodynamic self-diffusivity (e.g., Li *et al.*, 1996). The particle self-diffusivity is a second-order tensor defined in terms of the variance in the position of the designated particle centers from the unperturbed paths. The transverse component of the diffusivity tensor is given by the long-time limits of the ratios

$$D_{yy} = \frac{\langle Y^2(t)\rangle}{2t} = \frac{\langle X(t)Y(t)\rangle}{kt^2} = \frac{\langle X^2(t)\rangle}{\frac{2}{3}k^2t^3}, \tag{17}$$

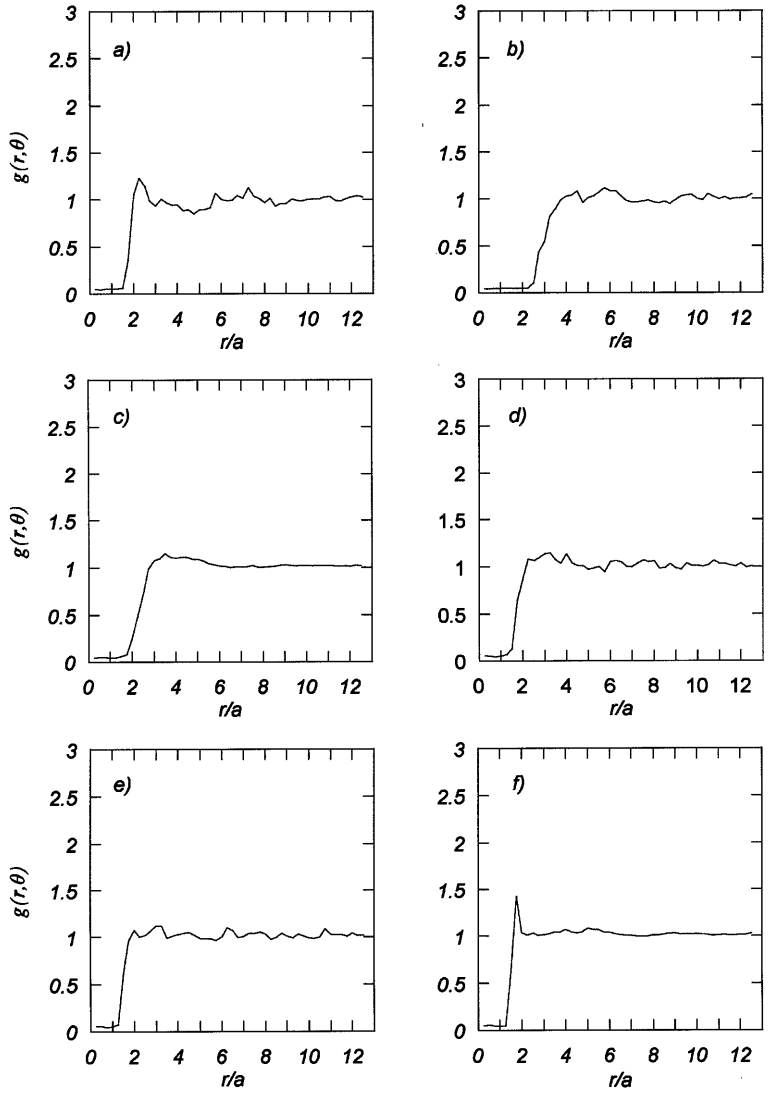

Figure 10. Same as Figure 9, but for elliptical capsules with unstressed axes ratio 0.5 corresponding to the suspension depicted in Figure 7(b).

where $X(t) = x(t) - x(0) + kty(t)$, $Y(t) = y(t) - y(0)$, and angular brackets signify averages over all particles. A similar diffusive motion is expected in the case of elastic capsules.

In Figure 11(a) we plot the three ratios shown in (17) for the suspension of circular unstressed capsules, and obtain strong evidence that the three values converge after statistical equilibrium has been established. Comparisons with the results of previous simulations shows that the diffusivity of capsules is higher than that of drops but lower than that of rigid particles at the same areal or volume fraction (Brady and Bossis, 1985; Li *et al.*, 1996). Suspensions of elliptical unstressed capsules show a similar behavior, as shown in Figure 11(b) for elliptical unstressed capsules of aspect ratio 0.5. It is interesting to note that the unstressed shape does not have a significant influence on the particle self-diffusivity, which suggests that the particle shape does not have a profound effect on the nature of the particle motion in a concentrated suspension.

To investigate the effect of capsule shape further, we conducted simulations of capsules with a biconcave unstressed shape, which is the counterpart of the biconcave discoidal shape assumed by red blood cells in the absence of flow. Figure 12 illustrates instantaneous interfacial profiles developing during the evolution. In this case the elastic membranes occasionally fold to produce irregular or even cusped shapes. Some of these shapes were confirmed to be physical, but others originate from numerical instabilities that could not be suppressed without substantial smoothing. Transient folding has been observed in previous simulations

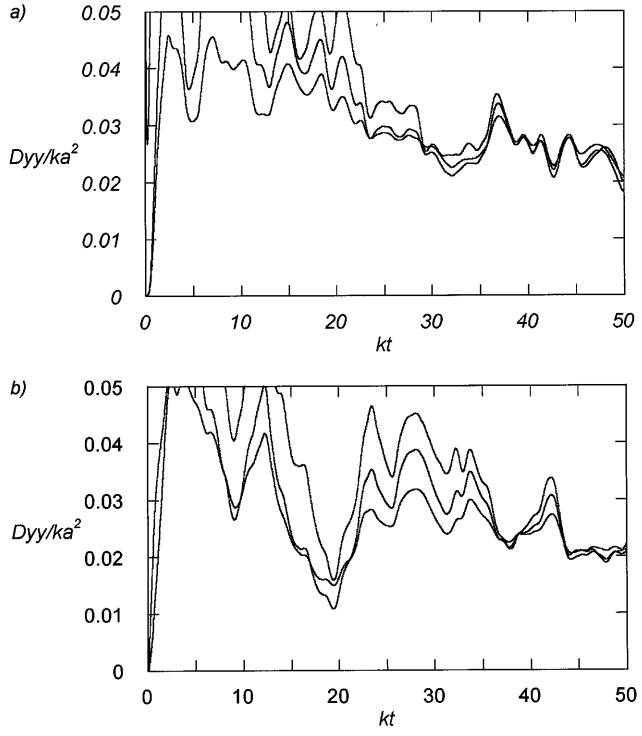

Figure 11. Evolution of the three ratios defining the capsule self-diffusivity corresponding to the suspensions depicted in Figure 7.

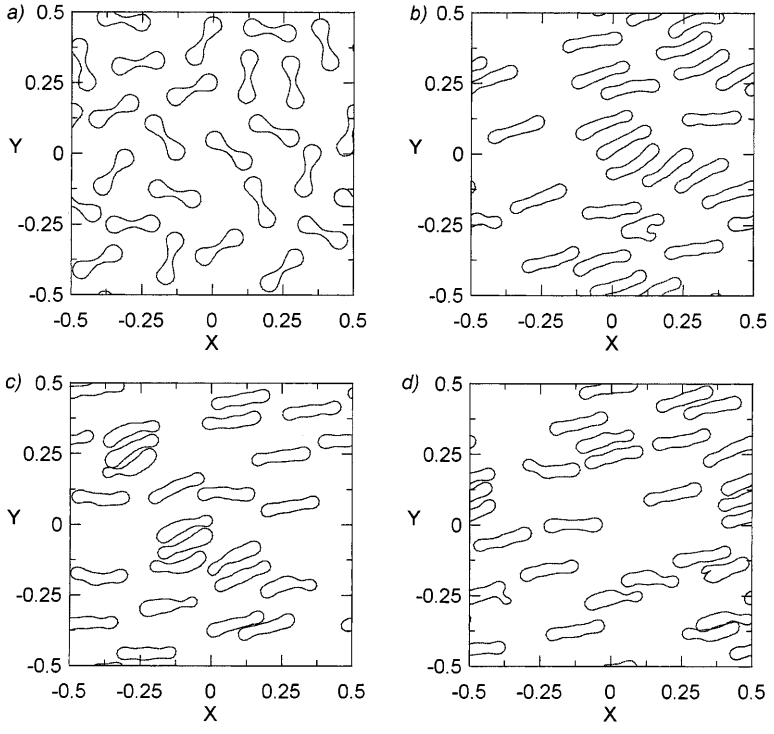

Figure 12. Interfacial profiles developing during the evolution of a suspension of 25 elastic capsules with biconcave unstressed shapes, at the areal fraction $\varphi = 0.20$, for $\Omega = 0.04$, at times (a) $kt = 0$, (b) 5, (c) 10, and (d) 15.

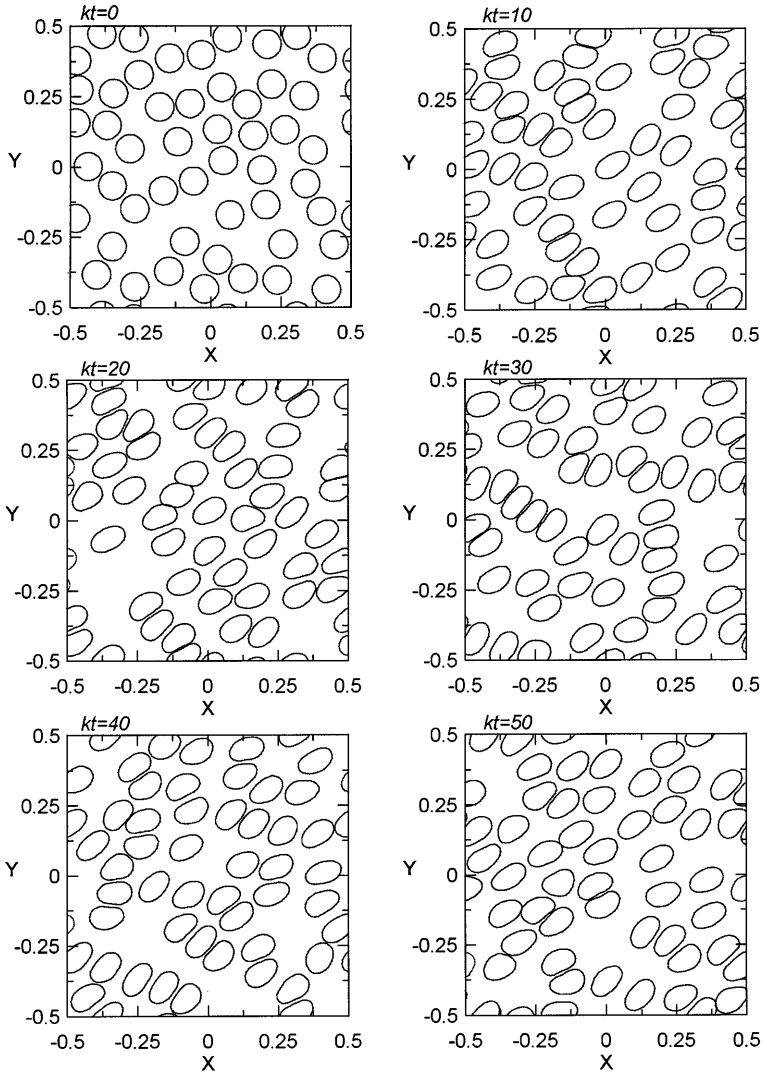

Figure 13. (a) Interfacial profiles developing during the evolution of a suspension of 50 elastic capsules with circular unstressed shapes, at the areal fraction $\varphi = 0.40$, for $\Omega = 0.005$, at times $kt = 0$, 10, 20, 30, 40, and 50.

of three-dimensional capsules with concave discoidal shapes (Pozrikidis, 1990; Ramanujan and Pozrikidis, 1998). Although the present simulations could not be sustained for an extended period of time, the rheological properties of the suspension for the duration of the simulation were found to be similar to those of suspensions of capsules with circular and elliptical shapes.

Next, we turn to examining the effect of the suspended phase areal fraction. At high areal fractions, numerical difficulties prevented us from carrying out extended simulations for capsules with noncircular unstressed shapes. Figure 13 shows a sequence of interfacial profiles for a suspension at the areal fraction $\varphi = 0.40$ and $\Omega = 0.005$. The most interesting new feature is the development of dimpled shapes between two strongly interacting particles due to the development of strong lubrication forces. Although the shapes of the interfaces are similar to those developing in suspensions of liquid drops, the structure of the flow is significantly different due to the tank-treading motion of the membranes.

In Figure 14(a), (b), we plot the evolution of the suspension effective viscosity and normal stress difference. The effective visocisty of an infinitely dilute suspension of rigid disks predicted by (16) is $\mu_{\text{eff}} = 1.8\mu$, which is substantially lower than the mean value arising from the simulations. Comparing these results to those shown with the solid lines in Figure 11 for $\varphi = 0.25$, we observe higher mean values and fluctuations with larger amplitudes. As in the case of rigid particles and liquid drops, the effective viscosity and normal

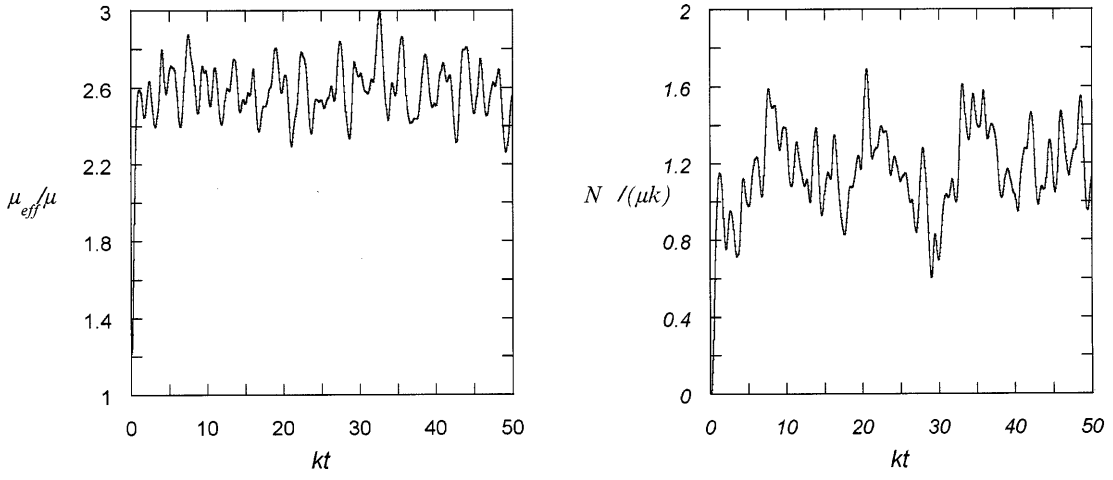

Figure 14. Evolution of the normalized suspension effective viscosity and normal stress difference for the suspension depicted in Figure 13.

stress difference increase monotonically with the areal fraction. The behavior on the limit of very high areal fractions is discussed in the next section.

The directional profiles of the pair distribution function g, shown in Figure 15, are similar to those shown in Figure 10 for $\varphi = 0.25$, and this suggests a weak dependency of the geometry of the microstructure on the suspended phase areal fraction. In Figure 16 we plot the three ratios defined in (17) and obtain strong evidence of a well-defined self-diffusivity whose value is approximately twice that for $\varphi = 0.25$. The estimated value for $\varphi = 0.40$ is substantially higher than that computed by Li *et al.* (1996) for liquid drops with constant interfacial tension, and this is attributed to the stronger hydrodynamic interactions causing larger displacements after interception.

6. Discussion

We have studied the deformation of solitary two-dimensional elastic capsules, the interaction between two intercepting capsules in infinite flow, and the rheological and statistical properties of a periodic suspension of elastic capsules in simple shear flow. Overall, the numerical results have suggested that the behavior of suspensions of capsules whose viscosity is equal to that of the ambient fluid is intermediate between that of drops and rigid particles studied by previous authors. Elastic capsules are deformable and thus liquid-drop-like, but since the onset of large velocity gradients along the interface is prevented by the development of elastic tensions, membrane tank-treading motion is established at equilibrium.

As the viscosity of a capsule is increased, the time scale of the capsule deformation is raised, and the capsule behaves increasingly more like a rigid particle, being able to execute complete rotation and undergoing flipping motion under the influence of a simple shear flow. When complete rotation becomes possible, the instantaneous distribution of the capsule orientation in a suspension of noninteracting capsules at low areal fractions is indeterminate, in the sense that it depends strongly on the initial orientation. It is possible that strong particle interactions in a dense suspension may lead to statistical equilibrium in which the particle orientation is described by a probability density distribution that is independent of the initial condition. Unfortunately, high computational cost prevented us from simulating suspensions of rigid-particle-like capsules corresponding to viscosity ratios sufficiently higher than unity. The simulation of such systems requires the development of more efficient algorithms.

The modulus of elasticity of the membrane of the red blood cells has been reported to have a broad range of values depending on the type of deformation, with a typical value being on the order of $E = 4 \times 10^{-3}$ dyn/cm (e.g., Skalak *et al.*, 1989). Using the values $\mu = 0.01$ dyn-sec/cm^2, and $a = 4 \times 10^{-4}$ cm, we find that when the shear rate k varies in the physiologically and experimentally relevant range 0.01–10^3 sec^{-1}, the dimensionless shear rate Ω varies in the range 10^{-5} and 1 which was considered in the present

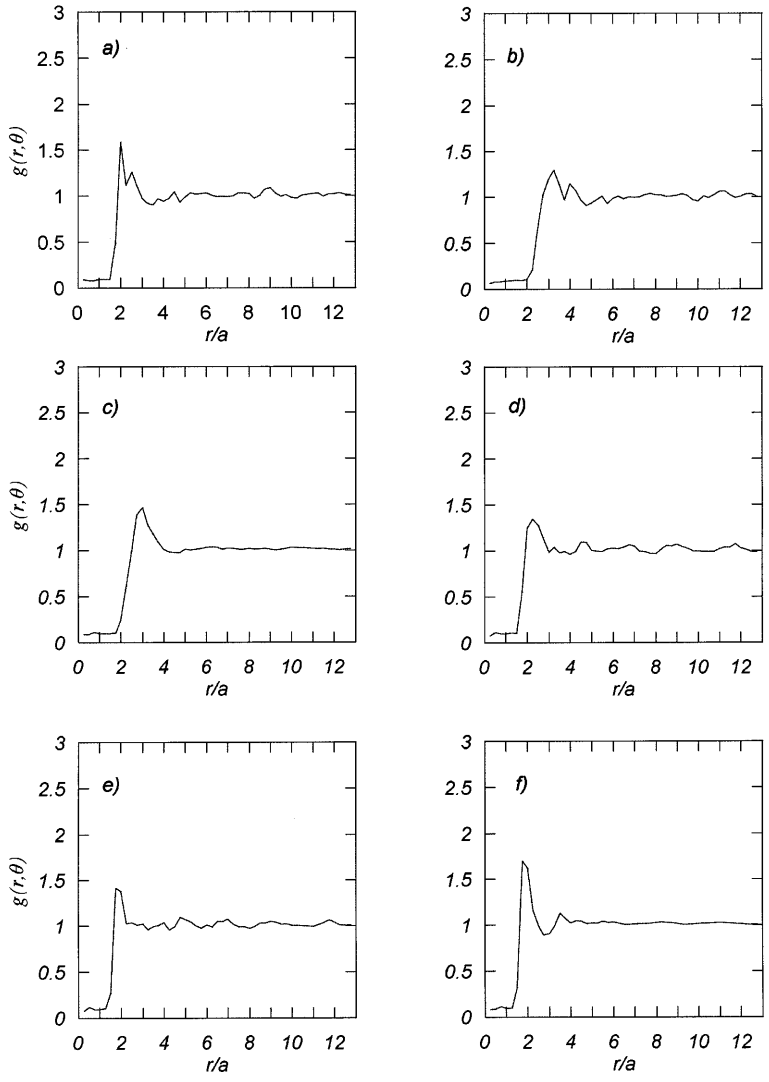

Figure 15. Pair-distribution function g plotted against the radial distance r/a for various angular directions corresponding to the suspension depicted in Figure 13; (a) $\theta = 0$, (b) $\pi/6$, (c) $\pi/3$, (d) $\pi/2$, (e) $2\pi/3$, and (f) $5\pi/6$.

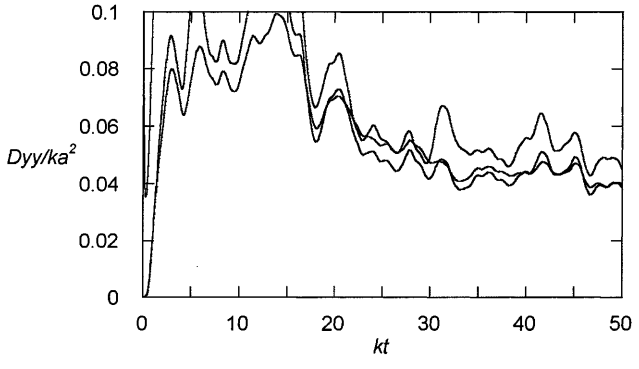

Figure 16. The evolution of the three ratios defining the capsule self-diffusivity corresponding to the suspension depicted in Figure 13.

simulations. Since, however, the viscosity of the cytoplasm can be as high as ten times the viscosity of the fluid in which the cells are suspended, caution should be exercised in interpreting the present results in the context of hemodynamics. Experiments on the deformation of red and other blood cells are often done in a buffer solution whose viscosity is comparable with that of the cytoplasm, and our results should be useful in interpreting these measurements.

Two additional considerations arise in interpreting the results of the present simulations for two-dimensional flow in the realistic context of three-dimensional blood flow. First, because of membrane incompressibility, cell elongation is accompanied by narrowing in the cross-flow direction, and this causes shearing deformation whose magnitude is determined by the shear modulus of elasticity. This type of deformation is overlooked in the two-dimensional model. More importantly, the tank-treading motion of a three-dimensional cell causes energy dissipation which raises the effective viscosity of the capsules and promotes a rigid-particle-like behavior (Fischer, 1980). As a result, red blood cells do not assume stationary shapes in shear flow unless the viscosity of the suspending medium is much higher than that of the plasma.

Blood is known to behave like a shear thinning medium with a yield-stress response at small shear rates (e.g., Fung, 1981). For example, as the shear rate is raised from 0.01 to 10^3 sec^{-1} in a Couette flow device, the apparent viscosity decreases by two orders of magnitude from 1 to 0.04 dyn-sec/cm^3. The drastic decrease in the range 0.01 to 10^2 sec^{-1} is due to the disintegration of cell aggregates developing spontaneously due to cell adhesion. Pronounced shear thinning at higher shear rates is typical of suspensions of deformable particles due to the ability of the cells to accommodate an incident flow by altering their shapes. At high volume fractions, healthy cells are able to slide over each other facilitated by the tank-treading motion, and this allows blood to flow even when the volume fraction of the red cells is as high as 0.95. At such high concentrations, blood assumes a foam-like configuration characterized by thin layers of fluid separated by adjacent membranes (Secomb *et al.*, 1983a,b). A similar behavior is expected in suspensions of elastic capsules presently considered at high shear rates.

The simulations of elastic capsules with circular unstressed shapes at the areal fraction 0.40 and dimensionless shear rate $\Omega = 0.005$ showed that the effective viscosity of the suspension is approximately 2.5 times that of the suspending fluid. This prediction is only slightly lower than laboratory measurements of blood at red blood cell volume fraction 0.40 and at sufficiently high shear rates so that cell aggregates are not present (Fung, 1981, p. 83). The differences in the computed and estimated values may be attributed to the different unstressed shapes, to the membrane incompressibily that has been neglected in the present model, to the higher viscosity of the cytoplasm, and, last but not least, to the present assumption of two-dimensional flow.

The development of computational models that allow the investigation of the significance of the membrane properties on the micro- and macrorheology of blood, has been a long-standing desire. In the present work we considered capsules enclosed by elastic membranes. A more comprehensive model would account for additional features including membrane incompressibility, membrane bending resistance, as well as particle aggregation at near contact. The incorporation of these features into a computational procedure is the subject of ongoing research.

References

Barthés-Biesel, D. (1980). Motion of a spherical microcapsule freely suspended in a linear shear flow. *J. Fluid Mech.*, **100**, 831–853.

Barthés-Biesel, D., and Rallison, J.M. (1981). The time-dependent deformation of a capsule freely suspended in a linear shear flow. *J. Fluid Mech.*, **113**, 251–267.

Barthés-Biesel, D., and Sgaier, H. (1985). Role of membrane viscosity in the orientation and deformation of a spherical capsule suspended in shear flow. *J. Fluid Mech.*, **160**, 119–135.

Batchelor, G.K. (1970). The stress system in a suspension of force-free particles. *J. Fluid Mech.*, **41**, 545–570.

Belzons, M., Blanc, R. Bouillot, J-L., and Camoin, C. (1981) Viscosité d'une suspension dilués et bidimnsionelle de sphères. *C. R. Acad. Sc. Paris Ser. II*, **292**, 939–944.

Boey, S.K., Boal, D.H., and Discher, D.E. (1998). Simulations of the erythrocyte cytoskeleton at large deformation. I. Microscopic models. *Biophys. J.*, **75**, 1573–1583.

Brady, J.F., and Bossis, G. (1985). The rheology of concentrated suspensions of spheres in simple shear flow by numerical simulation. *J. Fluid Mech.*, **155**, 105–129.

Charles, R., and Pozrikidis, C. (1998). Significance of the dispersed-phase viscosity on the simple shear flow of suspensions of two-dimensional liquid drops. *J. Fluid Mech.*, **365**, 205–234.

Cortez. R., and Varela, D.A. (1997). The dynamics of an elastic membrane using the impulse method. *J. Comput. Phys.*, **138**, 224–247.
Discher, D.E., Boal, D.H., and Boey, S.K. (1998). Simulations of the erythrocyte cytoskeleton at large deformation. II. Micropipette aspiration. *Biophys. J.*, **75**, 1584–1597.
Dold, J.W. (1992). An efficient surface-integral algorithm applied to unsteady gravity waves. *J. Comput. Phys.*, **103**, 90–115.
Edwards, D.A., Brenner, H., and Wasan, D.T. (1991). *Interfacial Transport Processes and Rheology*. Butterworth-Heinemann, Boston, Massachussets.
Eggleton, C.D., and Popel, A.S. (1998). Large deformation of red blood cell ghosts in a simple shear flow. *Phys. Fluids A.*, **10**, 1834–1845.
Fischer, T.M. (1980). On the energy dissipation in a tank-treading human red blood cell. *Biophys. J.*, **32**, 863–868.
Fung, Y.C. (1981). *Biomechanics; Mechanical Properties of Living Tissues*. Springer-Verlag.
Hansen, J.P., and McDonald, I.R. (1986). *Theory of Simple Liquids*. Academic Press.
Kennedy, M.R., Pozrikidis, C., and Skalak, R. (1994). Motion and deformation of liquid drops, and the rheology of dilute emulsions in simple shear flow. *Comput. Fluids*, **23**, 251–278.
Kraus, M., Wintz, W., Seifert, U., and Lipowsky, R. (1996). Fluid vesicles in shear flow. *Phys. Rev. Lett.*, **77**, 3685–3688.
Li, X., and Pozrikidis, C. (1999). Wall-bounded and channel flow of suspensions of liquid drops. *Int. J. Multiphase Flow*, in press.
Li, X.Z., Barthés-Biesel, D., and Helmy, A. (1988). Large deformations and burst of a capsule freely suspended in an elongational flow. *J. Fluid Mech.*, **187**, 179–196.
Li, X., Charles, R., and Pozrikidis, C. (1996). Simple shear flow of suspensions of liquid drops. *J. Fluid Mech.*, **320**, 395–416.
Lipowsky, R. (1991). The conformation of membranes. *Nature*, **349**, 475–481.
Loewenberg, M., and Hinch, E.J. (1996), Numerical simulation of a concentrated emulsion in shear flow, *J. Fluid Mech.*, **321**, 395–419,
Mohandas, N., and Evans, E. (1994) Mechanical properties of the red cell membrane in relation to molecular structure and genetic defects. *Annu. Rev. Biophys. Biomol. Struct.*, **23**, 787–818.
Navot, Y. (1998) Elastic membranes in viscous shear flow. *Phys.Fluids A.*, **10**, 1819–1833.
Pozrikidis, C. (1990). The axisymmetric deformation of a red blood cell in uniaxial straining flow. *J. Fluid Mech.*, **216**, 231–254.
Pozrikidis, C. (1992). *Boundary Integral and Singularity Methods for Linearized Viscous Flow*. Cambridge University Press, Cambridge.
Pozrikidis, C. (1994) Effects of surface viscosity on the deformation of liquid drops and the rheology of dilute emulsions in simple shearing flow. *J. Non-Newt. Fluid Mech.*, **51**, 161–178.
Pozrikidis, C. (1995). Finite deformation of liquid capsules enclosed by elastic membranes in simple shear flow. *J. Fluid Mech.*, **297**, 123—152.
Pozrikidis, C. (1996). Computation of periodic Greens functions of Stokes flow. *J. Eng. Math.*, **30**, 79–96.
Pozrikidis, C. (1997). *Introduction to Theoretical and Computational Fluid Dynamics*. Oxford University Press.
Pozrikidis, C. (2000). Interfacial dynamics for Stokes flow. *J. Comput. Phys.*, submitted.
Ramanujan, S., and Pozrikidis, C. (1998). Deformation of liquid capsules enclosed by elastic membranes in simple shear flow: large deformations and the effect of fluid viscosities. *J. Fluid Mech.*, **361**, 117–143.
Rosenkilde, C.E. (1967). Surface-Energy Tensors. *J. Math. Phys.*, **8**, 84–88.
Russel, W.B., Saville, D.A., and Schowalter, W.R. (1989). *Colloidal Dispersions*. Cambridge University Press, Cambridge.
Scriven, L.E. (1960). Dynamics of a fluid interface. *Chem. Eng. Sci.*, **12**, 98–108.
Secomb, T.W., Chien, S., Jan, K.-M., and Skalak, R. (1983a). The bulk rheology of close-packed red blood cells in shear flow. *Biorheology*, **20**, 295–309.
Secomb, T.W., Fischer, T.M., and Skalak, R. (1983b). The motion of close-packed red blood cells in shear flow. *Biorheology*, **20**, 283–294.
Seifert, U. (1998). Modelling nonlinear red cell elasticity. *Biophys J.*, **75**(3), 1141–1142.
Skalak, R., Özkaya, N., and Skalak, T.C. (1989). Biofluid mechanics. *Annu. Rev. Fluid Mech.*, **21**, 167–204.
van den Vorst, G.A.L. (1996). Integral formulation to simulate the viscous sintering of a two dimensional lattice of periodic unit cells. *J. Eng. Math.*, **30**, 97–118.
Zhou, H., and Pozrikidis, C. (1995). Deformation of liquid capsules with incompressible interfaces in simple shear flow. *J. Fluid Mech.*, **283**, 175–200.
Zinchenko, A.Z., and Davis, R.H. (1999). An efficient algorithm for hydrodynamical interaction of many deformable drops. *J. Comp. Phys.*, in press.